Critical Stripping Current Leads to Dendrite Formation on Plating in Lithium Anode Solid Electrolyte Cells

Jitti Kasemchainan[a,b], Stefanie Zekoll[a,b], Dominic Spencer Jolly[a], Ziyang Ning[a], Gareth O Hartley[a], James Marrow[a] and Peter G Bruce[a,b,c*]

[a]Department of Materials, University of Oxford, Parks Road, Oxford OX1 3PH, UK

[b]The Faraday Institution, Harwell Campus, Didcot OX11 0RA

[c]Department of Chemistry, University of Oxford, South Parks Road, Oxford OX1 3QZ, UK

*Email: peter.bruce@materials.ox.ac.uk

A critical current density on stripping (CCS) is identified that results in dendrite formation on plating and cell failure. When the stripping current density removes lithium from the interface faster than it can be replenished, voids form in the lithium at the interface and accumulate on cycling increasing the local current density at the interface and ultimately leading to dendrite formation on plating, short-circuit and cell death. This occurs even when the overall current density is significantly below the threshold for dendrite formation on plating. For the Li / Li_6PS_5Cl / Li cell, this is 0.2 and 1 $mA \cdot cm^{-2}$ at 3 and 7 MPa pressure respectively, compared with a critical current for plating of 2 $mA \cdot cm^{-2}$ at both 3 and 7 MPa. The pressure dependence on stripping indicates creep rather than Li diffusion is the dominant mechanism transporting Li to the interface. The critical stripping current is a major factor limiting the power density of lithium anode solid state cells. Significant pressure may be required to achieve even modest power densities in solid state cells.

Solid-state cells composed of a ceramic electrolyte and lithium metal anode have the potential to deliver enhanced safety along with higher specific energy and energy density compared with liquid electrolyte Li-ion batteries.[1] However, even 99 % dense ceramic electrolytes suffer from failure due to short-circuits arising from penetration of Li dendrites through the ceramic on plating.[11,12] For LLZO ($Li_7La_3Zr_2O_{12}$), the current density for dendrite formation can be as low as 0.6 $mA \cdot cm^{-2}$.[6,13,14] Another significant problem is that contact can be lost due to void formation between the solid electrolyte and Li during stripping.[15–23] It is difficult to separate plating from stripping with two electrode, Li/SE/Li cells.[21,24] A recent paper used 2-electrode cells in which one electrode was formed under very high pressure to minimize interfacial impedance, and highlighted the role of void formation in polarization on stripping.[25]

Here we use 3-electrode cells to study separately the processes of plating and stripping Li metal at the Li metal / Li_6PS_5Cl interface on cycling. Argyrodite, Li_6PS_5Cl, was chosen as the solid electrolyte. Sulphides have higher conductivity than oxides and are being pursued as the electrolyte of choice by a number of companies attempting to commercialise solid-state batteries.[27–30] Argyrodite has the advantage of being less brittle than the other highly conducting sulphides.[31] In addition, we show that it produces a kinetically stable interface with Li metal. By separating plating from stripping we demonstrate that each has a critical current density above which dendrite formation and short-circuiting will occur. When the current density on stripping is such that it exceeds the rate at which Li is replenished at the surface, voids form in the Li metal at the interface.[17,21] They are only partially eliminated on subsequent plating and hence voids accumulate on cycling, reducing the contact area at the interface and increasing the local current density. In such circumstances, even when the overall current density is lower than the threshold for dendrite formation on plating, the local current density will rise to exceed the limit for dendrite formation on plating, resulting in dendrite formation and short-circuiting. Increasing pressure increases the threshold of current density below which dendrites do not form, demonstrating that Li metal creep is the primary mechanism of replenishing Li metal at the interface. Although voltage polarisation is high on stripping, it

returns rapidly to a much lower value on subsequent plating due to rapid formation of a Li film across the electrolyte surface that occludes the voids formed on the previous stripping. Critical current density on stripping can be identified through single stripping experiments and can predict the threshold of current density below which dendrite formation will not occur and therefore at which cells can be cycled indefinitely. With a stack pressure of 3 MPa for Li / Li_6PS_5Cl, the maximum current for avoiding voids and subsequently dendrite formation is 0.2 $mA \cdot cm^{-2}$, rising to 1.0 $mA \cdot cm^{-2}$ at 7 MPa.

Li_6PS_5Cl (Argyrodite) was synthesised as described in the Methods section. The composition was confirmed by powder X-ray diffraction patterns which displayed the peaks characteristic of the Argyrodite structure, Fig. S1.[32] Disks were prepared by cold pressing the powder at 500 MPa, then loaded into a vacuum sealed quartz tube (< 10^{-5} mbar) before undergoing sintering at 300 °C for 15 minutes. The sintered disks were polished with a SiC abrasive disk with 1200 grit. All manipulations were carried out in an Ar filled glove box with a H_2O and O_2 content of < 1 ppm.

Two electrode cells were constructed by sandwiching the disk between two pieces of Li metal foil of 40 microns thickness, in order to investigate the stability of the interface. AC impedance data were collected as a function of time showing that the interfacial resistance (R_{SEI} + R_{CT}) stabilises with time, reaching within 10 % of the final value after 100 hours, Fig. S2. After contacting Li metal to the surface of our Li_6PS_5Cl disk for 250 h, the Li metal was removed and the surface of the disk investigated by phosphorus, sulfur and lithium XPS, Fig. S3. The XPS data demonstrate that the interface is dominated by the presence of Li_2S, with much smaller amounts of Li_3P and other compounds with the XPS signature of phosphosulphides. As expected, Li_6PS_5Cl is not stable in contact with Li metal,[33–35] however the electrolyte is reduced to compounds which are stable and ionic conductors (Li_2S), inhibiting further degradation and leading to a kinetically stable interfacial impedance.

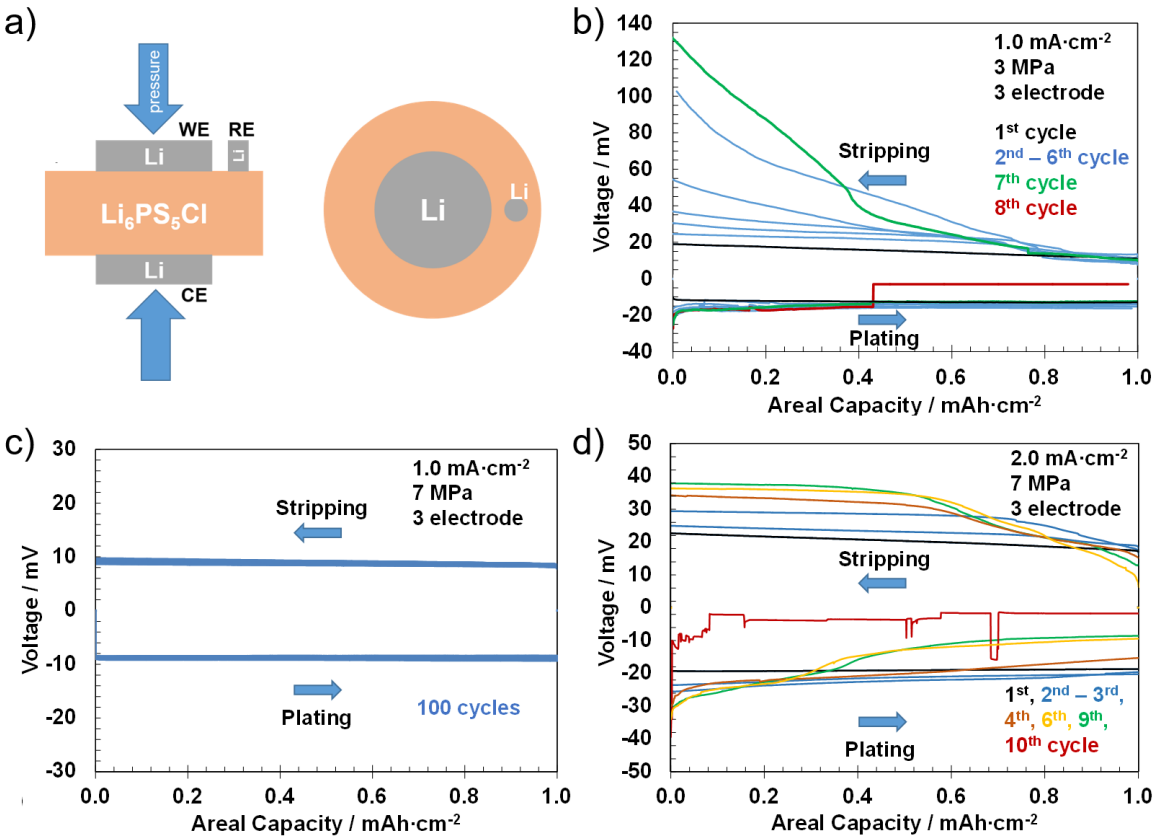

Figure 1 | Cell schematic and voltage vs charge passed for 3-electrode cells on Li metal plating and stripping at the Li / Li_6PS_5Cl interface: a) 3-electrode cell schematic b) 3 MPa – 1.0 mA·cm^{-2}, c) 7 MPa – 1.0 mA·cm^{-2}, d) 7 MPa – 2.0 mA·cm^{-2}.

The 3-electrode cells used Li foil for all three electrodes, working, counter and reference. A schematic of the cell configuration is shown in Fig. 1a. The cell was clamped under constant pressure, which was controlled as described in the Methods section. A constant current was passed between the working and counter electrodes with the potential of the working electrode being measured against the reference electrode.

Cycling 3-electrode cells under pressure of 3 MPa

A 3-electrode cell under a pressure of 3 MPa was cycled at a current density of 1 mA·cm^{-2} and capacity of 1 mAh·cm^{-2} (corresponding to approx. 5 microns of Li), representing realistic capacities and current densities. The variation of the working electrode potential with charge

passed is shown in Fig. 1 (b). It reveals a marked asymmetry in the polarisation between stripping and plating that could not have been identified from 2-electrode cell studies.[21] The cycling commenced with plating on the working electrode. The 1st plating occurs at a constant polarisation of 12 mV. Subsequent stripping begins with the same potential, but the potential then increases modestly and continuously with charge passed, reaching 19 mV at the end of stripping. With increasing cycle number, stripping polarisation increases, reaching a value of 130 mV at the end of the 7th stripping, Fig. 1 (b). In marked contrast, polarisation on plating remains small, averaging 13 mV. The cell short-circuits on the 8th cycle.

To assist in interpreting the severe asymmetry of polarisation, including the large polarisation on stripping, cells were cross-sectioned and subjected to SEM investigation, as described in the Methods section. The results are presented in Fig. 2 (a).

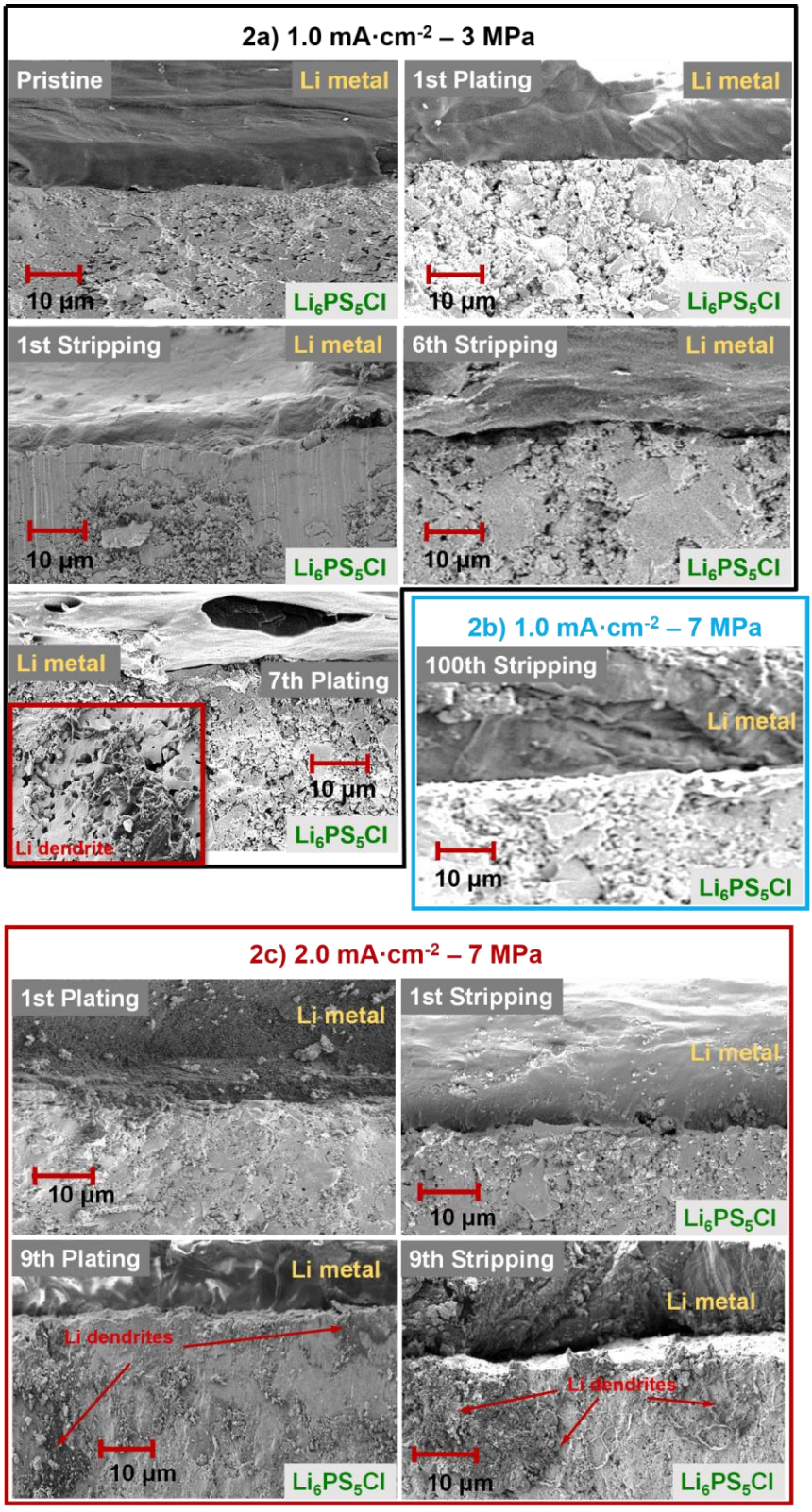

Figure 2 | Scanning Electron Microscopy (SEM) cross sections of the Li metal / Li_6PS_5Cl interface: a) 1.0 mA·cm^{-2} – 3 MPa; pristine, end of 1st plating, 1st stripping, 6th stripping, and 7th plating, b) 1.0 mA·cm^{-2} – 7 MPa; end of 100th stripping, c) 2.0 mA·cm^{-2} – 7 MPa; end of 1st plating, 1st stripping, 9th plating, and 9th stripping.

Stripping

The SEM images of the pristine working electrode / SE interface as well as after the 1st plating show that there is intimate and stable contact between the Li metal and the solid electrolyte. Some void formation is evident after the 1st stripping, in accord with the small rise in polarisation seen in Fig. 1 (b). In stark contrast, the SEM image at the end of the 6th stripping shows evidence of substantial detachment of the Li metal electrode from the solid electrolyte. Significant voids can be seen at the interface. The reduction of contact area between the Li metal and solid electrolyte results in an increase in local current density for the same constant overall current density (1 mA·cm^{-2}) and is in accord with the increasing polarisation observed on stripping. Support for the accumulation of voids at the interface on cycling comes from in-situ X-ray computed tomography of Li / Li_6PS_5Cl / Li cells, Fig. 3. The voids increase in number and length along the interface with increasing cycle number.

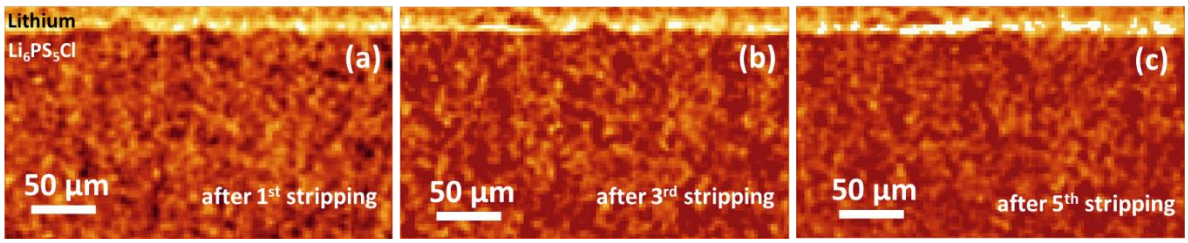

Figure 3 | In-situ X-ray computed tomography images of the Li metal / Li_6PS_5Cl interface of a Li metal / Li_6PS_5Cl / Li metal cell cycled: current density of 1.0 mA·cm^{-2} and capacity of 1.0 mAh·cm^{-2} (3 MPa) (a) after the 1st stripping, (b) after the 3rd stripping and (c) after the 5th stripping. The white pixels at the Li metal / Li_6PS_5Cl interface reveal the accumulation of voids (low X-ray attenuation) with increasing cycle number.

The generation of voids will occur when the stripping current removes Li from the interface faster than it can be replenished:

$J_{Li\ diffusion} + J_{Li\ creep} < J_{Li+\ migration}$, where J is the flux. The rate of Li transport to the interface depends on the diffusion of Li atoms within Li metal and Li metal creep.[36] As we shall see later, pressure-dependent measurements suggest creep rather than diffusion dominates the rate at which Li metal is replenished at the interface, although diffusion may play a more important role on initial stripping. As stripping proceeds on any given cycle, the inability of Li

to replenish as fast as it is removed by oxidation results in increasing voiding, increasing loss of Li / SE contact and increasing polarisation, as observed in Fig. 1 (b).

Plating

Turning to plating, given the high polarisation at the end of stripping after several cycles, how can the polarisation on plating be low? The SEM image at the end of the 7th plating shows that many of the voids present at the interface at the end of the previous, 6th, stripping are no longer present and that the contact area between Li metal and solid electrolyte has returned to be close to that observed in the 1st cycle (Fig. 2 (a)). This high degree of electrode / electrolyte contact agrees with the low value for polarisation on plating, and the observation that the plating polarisation for any given cycle remains close to the value of the 1st plating, despite the relatively high polarisation on stripping. While many voids are filled by the end of plating, this does not explain how the plating polarisation is low throughout the duration of most of the plating process on each cycle.

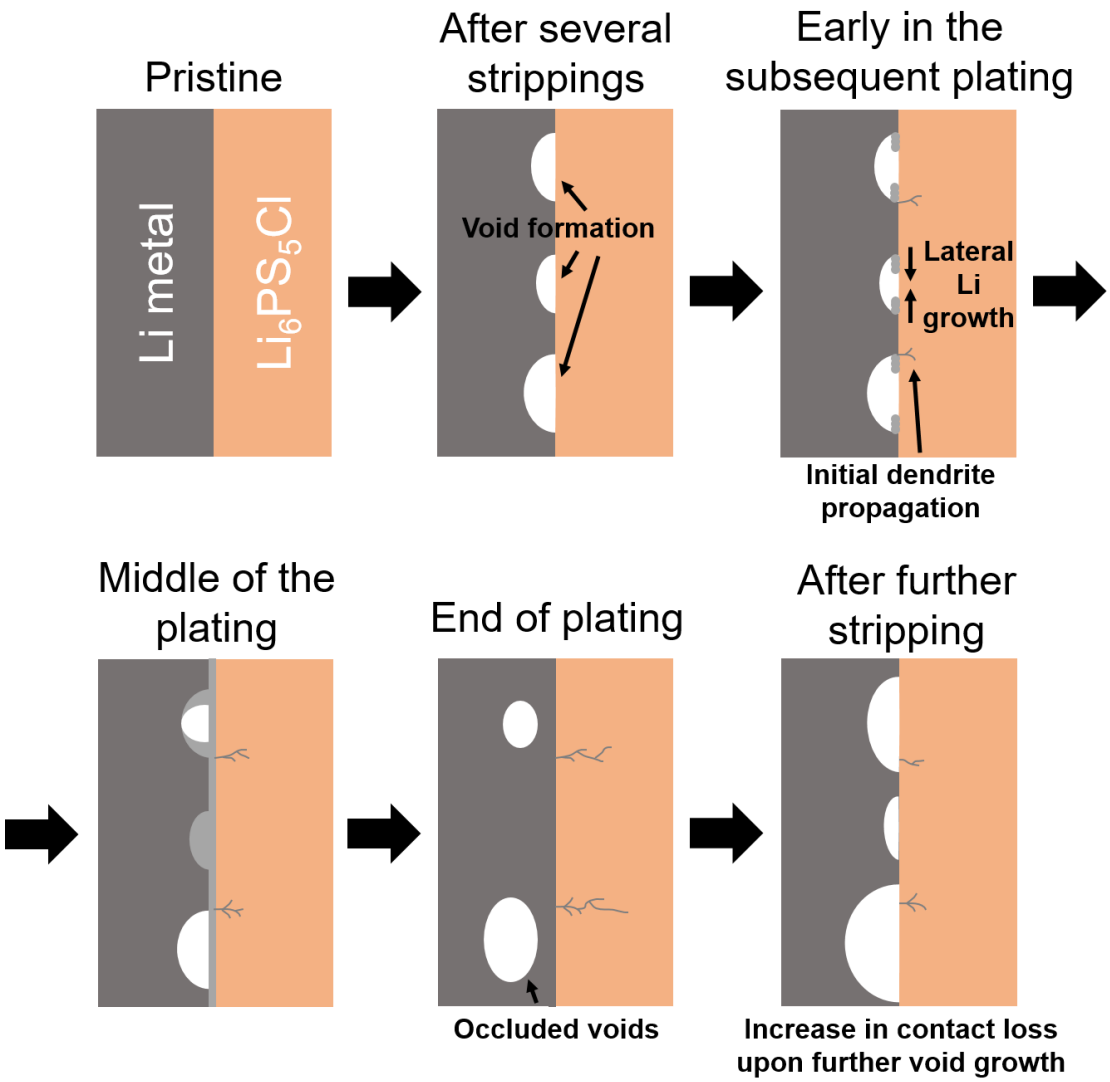

Figure 4 | Schematic of Li metal / Li_6PS_5Cl interface cycled at an overall current density above the critical current for stripping. Sequence from pristine to after several strippings and platings of Li metal: voids form on stripping, lateral growth of a thin Li film across the electrolyte surface (nucleating at where void edges meet the electrolyte) on subsequent plating results in low plating polarisation and formation of occluded voids. Some voids are eliminated on plating but the occluded voids reopen on subsequent stripping leading to accumulation of voiding and increasing loss of contact with cycling. This increases stripping polarisation and results in dendrites on plating.

Li deposition at the interface requires the simultaneous supply of Li^+ ions and electrons. Deposition commences where Li metal and solid electrolyte are in contact, but also where Li metal can grow unhindered. As a result, Li deposition will initiate at the triple point where Li metal, solid electrolyte and void meet, and then grow along the free surface of the void, as shown in Fig. 4. Growth of such a film cuts the voids off from the interface and they become occluded within the Li metal. It therefore requires only a relatively limited amount of charge

passed on plating to cover the solid electrolyte with a thin Li metal layer such that the area of contact is very similar to the pristine interface. This model predicts that in the very early stages of plating, the polarisation will drop rapidly as the layer grows laterally to cover the solid electrolyte surface. The model is in agreement with the experimental behaviour evident in Fig. 1 (b); explaining the observed rapid drop in polarisation in the early stages of plating and maintenance of a low polarisation thereafter as corresponding to the deposition of a 5 micron layer of Li filling many but not all of the voids. Those not filled become isolated and are forced away from the interface, Fig. 4. Such occluded voids are seen in the SEM image at the end of the 7^{th} plating (Fig. 2 (a)). We can now understand why the latter stages of plating and the initial stages of stripping both show low polarisation. The former is due to the intimate Li / SE contact resulting from the Li film that grows across the solid electrolyte surface. The latter arises because as stripping commences the Li / SE contact is the same as at the end of the previous plating. Only when the layer of Li in contact with the solid electrolyte is removed do the occluded voids become exposed to the solid electrolyte surface again, reducing the contact area and returning to the high polarisation.

The effect of cycling

The stripping polarisation increases with cycle number, because, as we have seen, not all voids formed on stripping are filled on the subsequent plating. Those that remain are occluded, as noted above, and become exposed at the interface with the solid electrolyte on the next stripping. As stripping proceeds, more voids also form and those already present grow in size, Fig. 4. In other words, the voids accumulate with cycle number, consistent with the increasing stripping polarisation with increasing cycle number. On initial plating, at these high cycle numbers, the local plating current density is high due to the poor Li / SE contact, resulting in dendrite formation, Fig. 4. Evidence of dendrite formation on the 7^{th} plating is in accord with the short circuit and cell failure on cycle 8.

Cycling 3-electrode cells under pressure of 7 MPa

To investigate the effect of pressure, the pressure on the 3-electrode cell was increased from 3 to 7 MPa. Results for plating and stripping are shown in Fig. 1 (c). The difference between 3 and 7 MPa is striking; plating and stripping at higher pressure proceed with almost no change in polarisation as a function of charge passed and with cycle number. The SEM images, Fig. 2 (b), show no evidence of voiding on stripping, with good conformal coating of Li across the solid electrolyte surface being maintained even after 100 cycles.

Increasing the current density from 1 to 2 $mA \cdot cm^{-2}$ while maintaining the higher pressure of 7 MPa changes the behaviour again, Fig. 1 (d). Initially, the cycling data are broadly similar to those at 3 MPa and a current density of 1 $mA \cdot cm^{-2}$. A modest rise in polarisation is observed on the 1st stripping consistent with some void formation at the interface, as seen in the SEM image in Fig. 2 (c). Stripping polarisation increases over the first few cycles while the plating polarisation soon returns to values close to that of the 1st plating. However, after those initial cycles the plating polarisation is reduced below that of the 1st plating and the onset of stripping on subsequent cycles exhibits polarisations that are less than the 1st stripping. Examination of the SEM images at the end of 9th plating show clear evidence of Li dendrites penetrating well into the solid electrolyte (Fig. 2 (c)). We interpret the reduction in polarisation at these higher cycle numbers as due to the dendrite penetration increasing the Li / SE interfacial area, but before the dendrites have fully propagated across the electrolyte resulting in a short-circuit. Under the conditions in Fig. 2 (c) this occurs after the 10th cycle.

Potential of Working and Counter electrodes during cycling

A 3-electrode cell was cycled and the voltage at the working and counter electrodes recorded simultaneously, confirming the overall similar behaviour at the working and counter electrodes, Fig. S4. During the first ½ cycle as Li is plated on the working electrode the polarisation of the counter rises due to stripping and thereafter the counter electrode exhibits a somewhat greater

polarisation than the working on cycling, in accord with greater void formation. Overall polarisation occurs and voids form at both electrodes and will contribute to dendrite formation from both electrodes. However, whether dendrites form on the working or counter electrode first in a Li symmetric cell is not a key issue, because in a full cell there is only one metal anode. What is important is that stripping above a critical current density causes the accumulation of voids, leading to the eventual formation of a dendrite, initiating at the Li anode, and cell failure.

Two Critical Currents One Plating and One Stripping

The implication of the above results is that both critical currents, the critical current for stripping (CCS) and the critical current for plating (CCP), can play a role in dendrite formation. CCS is defined as the current density above which Li is stripped faster than it is replenished at the Li / SE interface, resulting in void formation. If a cell is operated at a current density above CCS then there will be an increasing loss of contact between Li and the solid electrolyte on cycling, leading to increasing local current density for the same overall current density. If the critical current for dendrite formation on plating (CCP) is higher than CCS (which is the case here and is likely to be the case generally), then despite the overall current density being lower than the critical current for dendrite formation, dendrites, short circuit and cell failure are inevitable, it is only a question of how many cycles will be possible before failure. Of course if CCS > CCP then the former has no role in triggering dendrite formation.

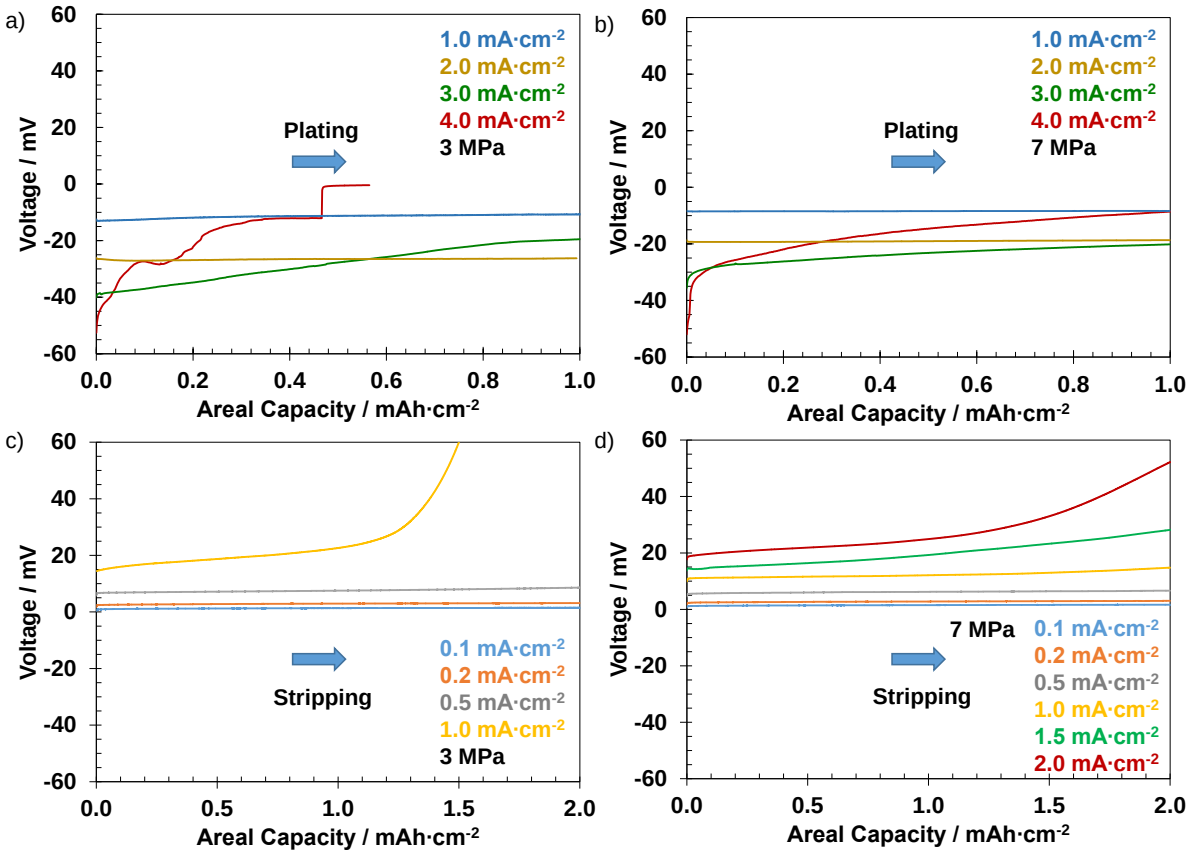

Figure 5 | Voltage vs charge passed for 3-electrode Li / Li_6PS_5Cl cells at different pressures and current densities: a) Plating at 3 MPa, b) Plating at 7 MPa, c) Stripping at 3 MPa, d) Stripping at 7 MPa

To explore the role of the critical currents further, 3-electrode cells were constructed and subjected to single plating and stripping at increasing current densities, Fig. 5. Considering plating, Fig. 5 (a) and (b), overall current densities on plating up to 2 mA·cm^{-2} are possible but 3 mA·cm^{-2} shows a reduction in polarisation with charge passed characteristic of dendrite formation, as shown in Fig. 1 (d). This is independent of pressure (same at 3 and 7 MPa, Fig. 5 (a) and (b)). On stripping, at the lower pressure of 3 MPa (Fig. 5 (c)), polarisation is severe at 1 mA·cm^{-2}, in accord with the results in Fig. 1 (b), whereas at 7 MPa (Fig. 5 (d)) the threshold is higher at 2.0 mA·cm^{-2}. These results are consistent with the importance of pressure on void formation, and as a result dendrite formation and cell short-circuiting. It should be noted that the pressures of 3 and 7 MPa are above the yield strength of Li, 0.81 MPa.[36] Despite this voids form. The generation of voids is a dynamic process driven by the stripping current, whereas

Li deformation/creep is expected to be relatively slow, favouring void formation. In addition it has been shown that voids can persist above the yield strength, where pressure deforms spherical voids into ellipsoidal voids rather than fully collapsing them.[37]

This effect of applying pressure below the yield strength of Li is seen in cycling a 3-electrode cell under a pressure of 0.5 MPa, below the yield strength of Li metal, 0.81 MPa.[38] At this pressure the absence of deformation made it a challenge to even form a cell. The data, Fig. S5, demonstrate that the polarisation decreases even on the 1st cycle, consistent with the interfacial contact improving on plating Li as well as in accord with dendrite growth due to the poor interfacial contact leading to high local current density at the interface. The subsequent stripping shows significant polarisation and the cell fails quickly. The SEM image after the final stripping shows very severe detachment of Li. In summary, at a pressure of 0.5 MPa, significantly below the yield strength of 0.81 MPa, the lack of Li deformation results in poor interfacial contact that worsens on cycling with rapid cell failure.

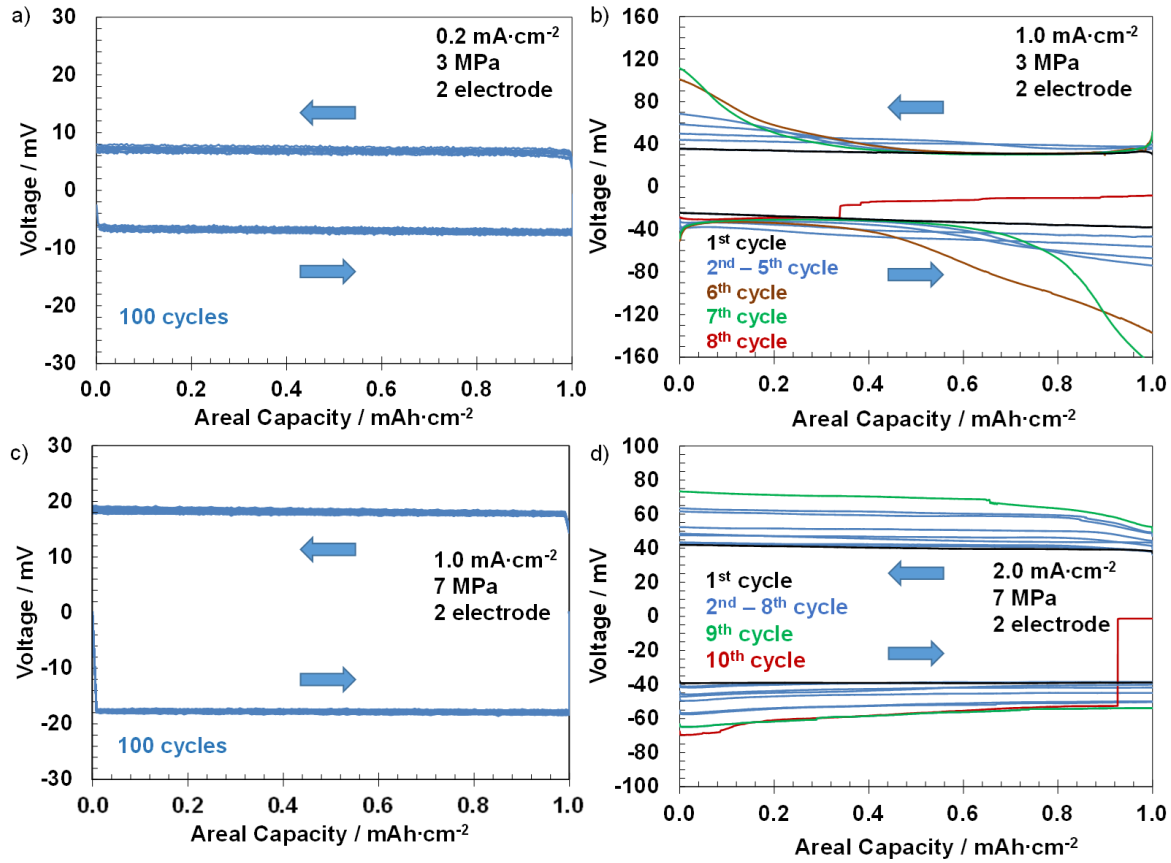

Figure 6 | Voltage vs charge passed for 2-electrode cells Li / Li_6PS_5Cl / Li cycled at different pressures and current densities: a) 3 MPa – 0.2 mA·cm^{-2}, b) 3 MPa – 1.0 mA·cm^{-2}, c) 7 MPa – 1.0 mA·cm^{-2}, d) 7 MPa – 2.0 mA·cm^{-2}

Two Electrode Cells

Based on the above results, 2-electrode cells, Li / SE / Li, were constructed and cycled below and above the CCS thresholds of 1 mA·cm^{-2} at 3 MPa and 2.0 mA·cm^{-2} at 7 MPa, Fig. 6. At a current density of 0.2 mA·cm^{-2} the cell at 3 MPa demonstrates continuous cycling with little change in polarisation. In contrast, at 1 mA·cm^{-2} the cell polarises and then short-circuits. At 7 MPa a current density of 1 mA·cm^{-2} does not result in any observable polarisation, whereas 2.0 mA·cm^{-2} is sufficient to generate dendrites and cell failure. AC impedance data were collected for 2-electrode cells cycled at 1 mA·cm^{-2} and 3 and 7 MPa respectively, Fig. S6. In accord with the data in Fig. 6, the impedance increased for the cells at 3 MPa, which demonstrated increased polarisation but not for the cells at 7 MPa, for which polarisation was constant on cycling.

The Li / Li_6PS_5Cl interface has been used in this work to investigate stripping and its effect on dendrite formation and cell failure. To illustrate that the results apply to other metal / solid electrolyte interfaces we have investigated Na / Na-β''-Alumina. Results identifying the critical current for stripping are shown in Fig. S7 along with cycling data above and below the critical current showing polarisation for the former and stable cycling for the latter. A more detailed study of the Na / Na-β''-Alumina interface is underway and will be reported in a later paper.

A consequence of the critical current for stripping is that it is very difficult to predict that a cell will cycle continuously without failure from cycling plots alone. If the overall current density is only marginally above CCS it may take many cycles for a cell to fail, and there may only be slight variations in polarisation during cycling, although fail it will. However, we suggest that the single stripping experiment shown in Fig. 5 (c) and (d) is a viable method for quantifying

the CCS at different pressures as it successfully predicts the current density above which void formation and dendrite penetration will occur for each pressure.

Critical current or potential

Voids form when the flux of Li^+ away from the areas of contact between Li and the solid electrolyte at the interface exceeds the flux of Li to the interface, i.e. above a critical local current density at the interface. The overall current density at which voids form will be the same as the critical current density at the interface provided there are no blocking layers at the interface resulting in constriction resistances. For simplicity we have assumed this is the case here. If however this is not the case then the overall current density for voids will be lower. The current density at the interface is linked intimately to the overpotential and the latter may be used as a criterion for dendrite formation.

If dendrite formation is to be avoided in all-solid-state cells, it is vital to cycle the cells below the critical current density at which voids begin to form at the Li metal / SE interface during stripping (CCS). This is the case even when the current density is below the threshold for dendrite formation on plating. When the current density is greater than CCS, voids accumulate on cycling, the Li / SE area of contact decreases correspondingly and as a result the local current density increases until it reaches a value where dendrites form on plating, leading to a short-circuit and cell death. It may take multiple cycles but cell failure is inevitable if the overall current density is greater than CCS. External pressure applied to cells during cycling is a key factor that governs CCS. Cycling at higher current density requires higher pressure in order to suppress formation of voids and hence ultimately dendrites. These results show that it is not just the current density for dendrite formation that is important in achieving cycling of all-solid-state cells at practical current densities, stripping currents are also important. Further possible factors such as surface chemistry, microstructure, adhesion, and mechanical

properties of both Li metal and solid electrolyte may warrant investigation as impacting the critical current density on stripping.

Methods

Synthesis of Li_6PS_5Cl

Li_2S, P_2S_5, and LiCl (Sigma-Aldrich) were ground together in the ratio corresponding to the stoichiometry of Li_6PS_5Cl. 1 g of powder was then loaded into a ZrO_2 ball-mill jar with 50 g of 10 mm diameter ZrO_2 balls. Two such sealed jars were placed in a Fritsch Pulverisette 7 premium line planetary micro mill and ball-milled at 600 rpm for 14 h. The resulting powder was pressed into a disk with a 5 mm diameter stainless steel die set under a uniaxial load of 1 tonne. The disk was sealed in an evacuated quartz tube surrounded by graphite foil as a supporting layer. The tube was placed inside a pre-heated box furnace at 600 ˚C for 15 min. then left to cool to room temperature. The disk was ground by mortar and pestle, and pressed into a 5 mm diameter disk at a uniaxial load of 1 tonne, sealed in a quartz tube as described previously and heated at 300 ˚C for 15 min. The sintered disk was cooled to room temperature and used to form the cells for electrochemical tests. All handling was performed inside an Ar-filled glovebox (O_2 and H_2O level < 1 ppm).

XRD

Powder X-ray diffraction (PXRD) was carried out using a Rigaku SmartLab X-ray diffractometer with Cu $K_{\alpha 1}$ radiation. Kapton tape was used to seal the powder from air. Patterns were collected from 10° to 70° in θ/2θ using a step-size of 0.01 at room temperature.

SEM

2- and 3-electrode cells were cross-sectioned using an ultrasonic cutter (Sonotec) with a tungsten carbide blade. The cross-sectioned cells were mounted on a custom-made holder with Cu adhesive tape and transferred into a Zeiss Merlin Scanning Electron Microscope (SEM) using an air-tight transfer device (Gatan).

X-ray computed tomography

The Li / Li_6PS_5Cl / Li cell was located within the chamber of a Zeiss Xradia Versa 510 X-ray computed tomography microscope. A Deben CT5000 loading rig was used to apply the pressure required for battery cycling. The cell was charged and discharged using a Gamry Interface 1010E inside the Xradia between scans.

XPS

X-ray Photoelectron Spectroscopy (XPS) was performed on the surface of sintered Li_6PS_5Cl disks using an ion pumped ultra-high vacuum (UHV) chamber fitted with a VG nine channel CLAM4 electron energy analyser. After leaving the Li_6PS_5Cl disk surface in contact with Li metal for 250 hours, the Li metal was carefully removed using a scalpel and the disk was attached onto Cu adhesive tape and transferred into the XPS chamber using a custom-built air-tight transfer device. CasaXPS software was used to fit the data. Elemental carbon at a binding energy of 384.8 eV was used as a reference.

Li / Li_6PS_5Cl / Li cell assembly

Metallic Li foil 200 µm thick was used for the electrodes. Any surface layer was removed with a scalpel. A 5 mm diameter disc of the Li foil was cut out and pressed at 10 tonnes, which reduced the foil's thickness to 40 µm. For the 2-electrode cell, two 2 mm diameter disc-shaped Li electrodes were cut from the foil and concentrically pressed onto both sides of a sintered Li_6PS_5Cl disk. In the case of the 3-electrode cell, a 0.5 mm diameter Li reference electrode

was additionally placed beside the working electrode. All cells were assembled and sealed under vacuum in pouch cells, with Cu foils serving as current collectors. Two different pressures (3 and 7 MPa) were applied to the pouch cells via spring clamps. The applied pressure was set and measured using a piezoelectric load cell (OMEGA).

Na / Na-β ”-Alumina / Na cell assembly

Discs of Na-β ”-Alumina 10 mm in diameter were obtained from Ionotec Ltd. The surfaces were prepared by polishing in deionised water with 400, 600, 1200 and 2500 grits of SiC paper. The discs were then heat treated at 400 °C in an Ar atmosphere. 100 µm thick metallic Na was used for the electrodes. Any film on the surface of the Na was removed with a scalpel immediately prior to cell assembly. 5 mm diameter discs were used as working and counter electrodes and a 1 mm diameter reference electrode was added for the 3-electrode cells. Cells were assembled and pressures were applied as for the Li / Li_6PS_5Cl / Li cells.

Galvanostatic cycling

Galvanostatic cycling was performed on the 2- and 3-electrode cells using a Gamry Interface-1000 device. The cycling areal capacity for each Li plating and Li stripping was fixed at 1.0 $mAh \cdot cm^{-2}$, which is equivalent to the plating and stripping of an approximately 5-µm-thick layer of Li metal.

EIS measurements

Electrochemical impedance spectroscopy was performed for 2-electrode cells at a voltage perturbation of 5 mV, in a frequency range from 1 MHz to 1 Hz using a Gamry Interface-1000 device. The data were analysed and fitted using the ZView software.

References

1. Hooper, A. & Tofield, B. C. All-solid-state batteries. *J. Power Sources* **11**, 33–41 (1984).

2. Kerman, K., Luntz, A., Viswanathan, V., Chiang, Y.-M. & Chen, Z. Review—Practical Challenges Hindering the Development of Solid State Li Ion Batteries. *J. Electrochem. Soc.* **164**, A1731–A1744 (2017).

3. Janek, J. & Zeier, W. G. A solid future for battery development. *Nat. Energy* **1**, (2016).

4. Zhou, W. *et al.* Polymer lithium-garnet interphase for an all-solid-state rechargeable battery. *Nano Energy* **53**, 926–931 (2018).

5. Pang, Q., Liang, X., Shyamsunder, A. & Nazar, L. F. An In Vivo Formed Solid Electrolyte Surface Layer Enables Stable Plating of Li Metal. *Joule* **1**, 871–886 (2017).

6. Cheng, E. J., Sharafi, A. & Sakamoto, J. Intergranular Li metal propagation through polycrystalline Li6.25Al0.25La3Zr2O12 ceramic electrolyte. *Electrochim. Acta* **223**, 85–91 (2017).

7. Nagao, M. *et al.* In situ SEM study of a lithium deposition and dissolution mechanism in a bulk-type solid-state cell with a Li2S-P2S5 solid electrolyte. *Phys. Chem. Chem. Phys.* **15**, 18600–18606 (2013).

8. Monroe, C. & Newman, J. The Impact of Elastic Deformation on Deposition Kinetics at Lithium/Polymer Interfaces. *J. Electrochem. Soc.* **152**, A396 (2005).

9. Monroe, C. & Newman, J. Dendrite Growth in Lithium/Polymer Systems. *J. Electrochem. Soc.* **150**, A1377 (2003).

10. Lotsch, B. V. & Maier, J. Relevance of solid electrolytes for lithium-based batteries: A realistic view. *J. Electroceramics* **38**, 128–141 (2017).

11. Porz, L. *et al.* Mechanism of Lithium Metal Penetration through Inorganic Solid

Electrolytes. *Adv. Energy Mater.* **7**, 1–12 (2017).

12. Swamy, T. *et al.* Lithium Metal Penetration Induced by Electrodeposition through Solid Electrolytes: Example in Single-Crystal Li 6 La 3 ZrTaO 12 Garnet. *J. Electrochem. Soc.* **165**, A3648–A3655 (2018).

13. Sharafi, A., Haslam, C. G., Kerns, R. D., Wolfenstine, J. & Sakamoto, J. Controlling and correlating the effect of grain size with the mechanical and electrochemical properties of Li7La3Zr2O12 solid-state electrolyte. *J. Mater. Chem. A* **5**, 21491–21504 (2017).

14. Sharafi, A. *et al.* Surface Chemistry Mechanism of Ultra-Low Interfacial Resistance in the Solid-State Electrolyte Li7La3Zr2O12. *Chem. Mater.* **29**, 7961–7968 (2017).

15. Botros, M., Djenadic, R., Clemens, O., Möller, M. & Hahn, H. Field assisted sintering of fine-grained Li7-3xLa3Zr2AlxO12 solid electrolyte and the influence of the microstructure on the electrochemical performance. *J. Power Sources* **309**, 108–115 (2016).

16. Yonemoto, F. *et al.* Temperature effects on cycling stability of Li plating/stripping on Ta-doped Li7La3Zr2O12. *J. Power Sources* **343**, 207–215 (2017).

17. Manalastas, W. *et al.* Mechanical failure of garnet electrolytes during Li electrodeposition observed by in-operando microscopy. *J. Power Sources* **412**, 287–293 (2019).

18. Basappa, R. H., Ito, T. & Yamada, H. Contact between Garnet-Type Solid Electrolyte and Lithium Metal Anode: Influence on Charge Transfer Resistance and Short Circuit Prevention. *J. Electrochem. Soc.* **164**, A666–A671 (2017).

19. Koerver, R. *et al.* Chemo-mechanical expansion of lithium electrode materials-on the route to mechanically optimized all-solid-state batteries. *Energy Environ. Sci.* **11**, 2142–2158 (2018).

20. Koerver, R. *et al.* Capacity Fade in Solid-State Batteries: Interphase Formation and Chemomechanical Processes in Nickel-Rich Layered Oxide Cathodes and Lithium Thiophosphate Solid Electrolytes. *Chem. Mater.* **29**, 5574–5582 (2017).

21. Koshikawa, H. *et al.* Dynamic changes in charge-transfer resistance at Li metal/Li7La3Zr2O12interfaces during electrochemical Li dissolution/deposition cycles. *J. Power Sources* **376**, 147–151 (2018).

22. Jow, T. R. & Liang, C. C. Interface Between Solid Electrode and Solid Electrolyte - A Study of the Li/LiI(AI2O3) Solid-Electrolyte System. *J. Electrochem. Soc.* **130**, 737–740 (1983).

23. Jow, T. R. & Liang, C. C. Interface between Solid Anode and Solid Electrolyte - Effect of Pressure on Li/LiI(Al2O3) Interface. *Solid State Ionics* 695–698 (1983).

24. Han, F. *et al.* High electronic conductivity as the origin of lithium dendrite formation within solid electrolytes. *Nat. Energy* (2019). doi:10.1038/s41560-018-0312-z

25. Krauskopf, T., Hartmann, H., Zeier, W. G. & Janek, J. Toward a Fundamental Understanding of the Lithium Metal Anode in Solid-State Batteries - An Electrochemo-Mechanical Study on the Garnet-Type Solid Electrolyte Li6.25Al0.25La3Zr2O12. *Appl. Interfaces Mater.* 14463–14477 (2019). doi:10.1021/acsami.9b02537

26. Han, X. *et al.* Negating interfacial impedance in garnet-based solid-state Li metal batteries. *Nat. Mater.* **16**, 572–579 (2017).

27. Zhang, Z. *et al.* New horizons for inorganic solid state ion conductors. *Energy Environ. Sci.* **11**, 1945–1976 (2018).

28. Zheng, F., Kotobuki, M., Song, S., Lai, M. O. & Lu, L. Review on solid electrolytes for all-solid-state lithium-ion batteries. *J. Power Sources* **389**, 198–213 (2018).

29. Kato, Y. *et al.* High-power all-solid-state batteries using sulfide superionic conductors. *Nat. Energy* **1**, 16030 (2016).

30. Zhou, L. *et al.* Solvent-Engineered Design of Argyrodite Li 6 PS 5 X (X = Cl, Br, I) Solid Electrolytes with High Ionic Conductivity. *ACS Energy Lett.* **4**, 265–270 (2019).

31. Deng, Z., Wang, Z., Chu, I.-H., Luo, J. & Ong, S. P. Elastic Properties of Alkali Superionic Conductor Electrolytes from First Principles Calculations. *J. Electrochem. Soc.* **163**, A67–A74 (2016).

32. Yu, C., van Eijck, L., Ganapathy, S. & Wagemaker, M. Synthesis, structure and electrochemical performance of the argyrodite Li6PS5Cl solid electrolyte for Li-ion solid state batteries. *Electrochim. Acta* **215**, 93–99 (2016).

33. Wenzel, S., Sedlmaier, S. J., Dietrich, C., Zeier, W. G. & Janek, J. Interfacial reactivity and interphase growth of argyrodite solid electrolytes at lithium metal electrodes. *Solid State Ionics* **318**, 102–112 (2018).

34. Wu, E. A. *et al.* New Insights into the Interphase between the Na Metal Anode and Sulfide Solid-State Electrolytes: A Joint Experimental and Computational Study. *ACS Appl. Mater. Interfaces* **10**, 10076–10086 (2018).

35. Zhu, Y., He, X. & Mo, Y. Origin of Outstanding Stability in the Lithium Solid Electrolyte Materials: Insights from Thermodynamic Analyses Based on First-Principles Calculations. *ACS Appl. Mater. Interfaces* **7**, 23685–23693 (2015).

36. Wang, M., Wolfenstine, J. B. & Sakamoto, J. Temperature Dependent Flux Balance of the Li/Li7La3Zr2O12 Interface. *Electrochim. Acta* **296**, 842–847 (2019).

37. Nemat-Nasser, S. & Hori, M. Void collapse and void growth in crystalline solids. *J. Appl. Phys.* **62**, 2746–2757 (1987).

38. Masias, A., Felten, N., Garcia-mendez, R., Wolfenstine, J. & Sakamoto, J. Elastic, plastic, and creep mechanical properties of lithium metal. *J. Mater. Sci.* **54**, 2585–2600 (2019).

Acknowledgements

P.G.B. is indebted to the Engineering and Physical Sciences Research Council (EPSRC), including the SUPERGEN Energy Storage Hub [EP/L019469/1], Enabling Next Generation Lithium Batteries [EP/M009521/1], the University of Oxford experimental equipment upgrade [EP/M02833X/1], Henry Royce Institute for capital equipment [EP/R010145/1] and the Faraday Institution All-Solid-State Batteries with Li and Na Anodes [FIRG007, FIRG008] for financial support. The authors thank Dr. Phil Holdway, Oxford Materials Characterisation Service, for help with XPS measurements.

Author Contributions

J.K. contributed to all aspects of the research. S.Z. performed the scanning electron microscopy experiments and analysed the data. D.S.J. performed electrochemical experiments and analysed the data. Z.N. performed synthesis of Li_6PS_5Cl and in-situ tomography experiments. P.G.B., J.K., S.Z., D.S.J., Z.N., G.O.H. and J.M. interpreted the data. P.G.B. wrote the paper with contributions from J.K., S.Z., D.S.J., Z.N. and G.O.H. The project was supervised by P.G.B.

Competing Financial Interests

The authors declare no competing financial interests.

Date Availability Statement

Supporting research data has been deposited in the Oxford Research Archive and is available under this DOI: